Published in final edited form as:
Acta Biomater. 2014 October ; 10(10): 4367–4376. doi:10.1016/j.actbio.2014.06.021.

Static Axial Stretching Enhances the Mechanical Properties and Cellular Responses of Fibrin Microthreads

Jonathan M. Grasman[1,2], **Laura Pumphrey**[1], **Melissa Dunphy**[1], **James Perez-Rogers**[1], and **George D. Pins**[1,2]

[1]Biomedical Engineering Department, Worcester Polytechnic Institute, Worcester, Massachusetts 01609

[2]Bioengineering Institute, Worcester Polytechnic Institute, Worcester, Massachusetts 01609

Abstract

Fibrin microthreads are a platform technology that can be used for a variety of applications, and therefore the mechanical requirements of these microthreads differ for each tissue or device application. To develop biopolymer microthreads with tunable mechanical properties, we analyzed fibrin microthread processing conditions to strengthen the scaffold materials without the use of exogenous crosslinking agents. Fibrin microthreads were extruded, dried, rehydrated, and static axially stretched 0-200% of their original lengths; then the mechanical and structural properties of the microthreads were assessed. Stretching significantly increased the tensile strength of microthreads threefold, yielding scaffolds with tensile strengths and stiffnesses that equaled or exceeded values reported previously for carbodiimide crosslinked threads without affecting intrinsic material properties such as strain hardening or Poisson's ratio. Interestingly, these stretching conditions did not affect the rate of proteolytic degradation of the threads. The swelling ratios of stretched microthreads decreased, and scanning electron micrographs showed increases in grooved topography with increased stretch, suggesting that stretching may increase the fibrillar alignment of fibrin fibrils. The average cell alignment with respect to the longitudinal axis of the microthreads increased twofold with increased stretch, further supporting the hypothesis that stretching microthreads increases the alignment of fibrin fibrils on the surfaces of the scaffolds. Together, these data suggest that stretching fibrin microthreads generates stronger materials without affecting their proteolytic stability, making stretched microthreads ideal for implantable scaffolds that require short degradation times and large initial loading properties. Further modifications to stretched microthreads, such as carbodiimide crosslinking, could generate microthreads to direct cell orientation and align tissue deposition, with additional resistance to degradation for use as a long-term scaffold for tissue regeneration.

Address Correspondence to: George D. Pins, PhD, Department of Biomedical Engineering, Worcester Polytechnic Institute, Worcester, MA 01609, Tel: 1-508-831-6742; Fax: 1-508-831-5541, gpins@wpi.edu.

Disclosures: GDP discloses that he is a co-founder and has an equity interest in Vitathreads L.L.C., a company that has licensed intellectual property associated with fibrin microthreads.

Keywords

tissue engineering; fibrin; microthreads; scaffolds; cell alignment

1. Introduction

Biopolymer microthreads are a platform technology that can be used for several applications including scaffolds for tissue engineering, delivery vehicles for growth factors or cells, or as suture materials. These microthreads can be composed of a variety of materials, including collagen [1-3], silk [4-6], or fibrin [7, 8]. The mechanical requirements of these microthreads vary for each tissue or device application. For example, scaffolds implanted into load-bearing tissues such as skeletal muscle require that the constructs provide provisional mechanical stability to the tissue in the wound site until native tissue is regenerated [9]. Conversely, a delivery vehicle for growth factors or cells may require relatively large initial mechanical loads to implant into the wound site, but require rapid degradation to facilitate controlled release of the specific growth factor or cell type. Therefore, there is a significant need to tune or modulate the mechanical properties of these materials during the microthread fabrication process to enable the design of function-specific microthread scaffolds.

Fibrin has been used extensively as a scaffold material in tissue engineering because of its intrinsic bioactivity and its role as a provisional matrix during the initial stage of wound healing [10, 11]. Fibrin is a branched, microfibrillar polymer, formed when activated thrombin cleaves two small peptides from fibrinogen, allowing fibrinogen to self-assemble into a complex fibrillar network. Fibrin gels have been shown to increase cell production of extracellular matrix proteins when compared to extracellular matrix protein production in cell-seeded collagen gels [12]. The molecular structure of fibrin enables individual microfibrils within the microfibrillar networks to undergo reorganization under tension, with strain at failure values in excess of 200% [13]. Another study demonstrated that the increase in tensile strength of stretched bulk fibrin scaffolds increased the alignment of the fibrin polymer network within the matrix [14]. Together these findings support the hypothesis that stretching of microfibrillar fibrin networks during scaffold fabrication will increase the organization and alignment of the polymer-like network and enhance the mechanical strength of the scaffold.

Our laboratory developed a novel technique to extrude dense fibrin scaffolds into microthreads with average diameters between 100 and 150 μm [15]. One advantage of these biopolymer microthreads is that their cylindrical shape facilitates cellular alignment and new tissue deposition along the longitudinal axis of the microthread, enabling the guided regeneration of tissues with aligned fibrous tissue organization such as skeletal muscle, tendon, or ligament. Another advantage of creating microthreads from a dense fibrin matrix is to increase the mechanical strength of the overall fibrin scaffold [15]. To further augment the mechanical properties of fibrin microthreads, we have investigated UV crosslinking [15], and carbodiimide crosslinking [16] methods to enhance the tensile strength of fibrin microthreads, and showed that carbodiimide crosslinking increased the tensile strength of microthreads as well as their resistance to proteolytic degradation *in vitro*. The current fibrin

microthread fabrication process involves stretching microthreads immediately after fibrin polymerization, which generates uniform scaffolds with repeatable structural properties; however, we are not aware of any systematic studies that analyze the effects of static axial stretching on the structural or functional properties of fibrin scaffolds, including fibrin microthreads.

The goal of the present study is to quantitatively characterize the effect of static axial stretching on the mechanical, structural, and biochemical properties of fibrin microthreads. We stretched fibrin microthreads 0-200% of their original lengths and evaluated their uniaxial strengths, rates of proteolytic degradation, and the degree with which C2C12 myoblasts aligned along the longitudinal axes of the microthreads. The results show that while stretching decreases the diameters of fibrin microthreads, it significantly increases the tensile strength and stiffness of the microthreads without affecting their rate of proteolytic degradation. The ability to tune the mechanical properties of fibrin microthreads without the use of crosslinking agents will create a more robust scaffold material that can be strategically employed as a regenerative matrix for tissues with varying mechanical and structural properties.

2. Materials and Methods

2.1. Fibrin Microthread Preparation

2.1.1. Microthread Extrusion—Fibrin microthreads were co-extruded from solutions of fibrinogen and thrombin using extrusion techniques described previously [15, 16]. Briefly, fibrinogen from bovine plasma (Sigma, St. Louis, MO; F8630) was dissolved in HEPES (N-[2-Hydroxyethyl]piperazine-N′-[2-ethanesulfonic acid]) buffered saline (HBS, 20 mM HEPES, 0.9% NaCl; pH 7.4) at 70 mg/mL and stored at -20 °C until use. Thrombin from bovine plasma (Sigma; T4648) was dissolved in HBS at 40 U/mL and stored at -20 °C until use.

To fabricate microthreads, fibrinogen and thrombin solutions were thawed and warmed to room temperature, and thrombin was mixed with a 40 mM $CaCl_2$ (Sigma) solution to form a working solution of 6 U/mL. Equal volumes of fibrinogen and thrombin/$CaCl_2$ solutions were loaded into separate 1 mL syringes which were inserted into a blending applicator tip (Micromedics Inc., St. Paul, MN; SA-3670). The solutions were combined in the blending applicator and extruded through polyethylene tubing (BD, Sparks, MD) with an inner diameter of 0.86 mm into a bath of 10 mM HEPES (pH 7.4) in a Teflon coated pan at a rate of 0.225 mL/min using a dual syringe pump.

2.1.2. Static Axial Stretching with and without a Drying Phase—Microthreads were incubated in 10 mM HEPES buffer for 10 minutes to facilitate fibrin polymerization, then the scaffolds were carefully removed from the bath solution without additional deformation and dried on a custom-made stretching device overnight (Figure 1A). After drying, threads were rehydrated in deionized water for one hour and static axially stretched to either 0, 50, 75, 100, 125, 150, 175 or 200 percent of their initial length. To analyze the contribution of the drying phase on the mechanical properties of stretched microthreads, batches of threads were also stretched immediately after polymerization to the desired

percentage (Figure 1B). After stretching, all threads were hung to dry under the tension of their own weight. Stretch percentages were reported as the ratio between the deformation (ΔL) of the thread and the starting length (L_0) of the thread (stretch % = $\Delta L/L_0$ *100%). Microthreads were fabricated using previously reported methods, which included static axial stretching of approximately 150% immediately after polymerization to form three 19 cm microthreads [16]. Hence these threads were designated as control threads. Dry, stretched threads were placed in aluminum foil and stored in a desiccator at room temperature until use.

2.2. Mechanical Characterization of Stretched Fibrin Microthreads

Mechanical characterization of stretched fibrin microthreads was performed using techniques described previously [16]. Briefly, individual microthreads were affixed with medical grade silicone adhesive to vellum paper frames with precut windows that defined the region of loading. An initial gage length of 2.0 cm was defined as the distance between adhesive spots at the edges of the precut window in the vellum frame. The microthreads on the vellum frames were hydrated in phosphate buffered saline (PBS) for at least 60 minutes prior to testing. Hydrated microthread diameters were measured using a calibrated reticule with a 10X objective, coupled to a Nikon Eclipse E600 upright microscope (Melville, NY). Microthreads were assumed to be cylindrical, and the diameter was determined by averaging 3 measurements taken along the length of each microthread to define the cross-sectional area. After hydration, microthreads were securely mounted in the grips of a uniaxial testing machine (ElectroPuls E1000; Instron, Norwood, MA) and a 1 N load cell, the edges of each vellum frame were cut, and the microthreads were uniaxially loaded until failure at a 50% strain rate (10 mm/min). Force and displacement were recorded continuously throughout each test at a frequency of 10 Hz. The mechanical failure load of each thread was recorded as the point where a rapid (80%) drop from the maximum load occurred. The grip-vellum paper interface was visually inspected during each test to ensure that no slippage occurred. Threads that slipped in the grips during testing were excluded from further analysis. Engineering stress was calculated as the amount of force detected by the load cell divided by the initial cross-sectional area. Strain was calculated as the increased extension from the gage-length.

A MATLAB (MathWorks, Natick, MA) script was written to analyze the ultimate tensile strength (UTS), initial thread modulus, maximum tangent modulus (MTM), strain at failure (SAF), and load at failure for each sample (Figure 2A). The initial modulus was defined as the initial linear region of the stress-strain curve, typically within the toe region. The MTM was defined as the highest linear region in the stress-strain curve for each sample over a moving window length corresponding to 20% of the total length of each test) and fitted to a linear region of the stress-strain curve. The strain hardening ratio was defined as the ratio between the MTM and the initial modulus. In the event that there was no change in the slope of the stress-strain curve (i.e. no visible toe region), the initial modulus was equal to the MTM and these values were not used to calculate strain hardening. Statistical analysis was used to identify and remove outliers as defined by microthreads whose wet diameters were 1.5 times greater than the inner quartile range (IQR) for each sample set (average wet diameter ± 1.5 *IQR). To ensure this method was robust, we determined that the distribution

of wet diameter measurements was normal using SigmaPlot 11.0 software (Systat Software, Inc., San Jose, CA) to validate our definition, and exclusion, of outliers. Data points falling outside of this range were excluded from later statistical analysis.

2.3. Structural Characterization of Stretched Fibrin Microthreads

2.3.1 Scanning Electron Microscopy—Fibrin microthreads were imaged with a scanning electron microscope (SEM) to characterized thread morphology and surface topography. Air-dried fibrin threads were mounted on aluminum stubs (Ted Pella, Redding, CA) coated with double-sided carbon tape and sputter coated with a thin layer of gold-palladium for 30 seconds at 45 mA using an EMS 550 (Electron Microscopy Sciences, Hatfield, PA). Images were acquired at 20 kV with a JSM-KLG SEM.

2.3.2. Thread Swelling—Prior to mechanical testing, the diameters of dry crosslinked microthreads were recorded using a calibrated reticule with a 10× objective. In each case, the diameter for each microthread was averaged from three measurements taken along the length. The wet diameter measurements taken during the mechanical testing procedure were also used to calculate the swelling ratio which was defined as the ratio of the wet diameter of a microthread to its dry diameter (wet/dry diameter).

2.3.3. Transverse Strain and Poisson Ratio Calculations—Transverse strain (diameter strain) was calculated as the change in the mean wet diameter of each stretched microthread with respect to the mean diameter of the unstretched microthreads. Poisson's ratio was determined to be the negative of the ratio between the transverse strain and the axial strain of microthreads after stretching (Poisson = - transverse strain / axial strain).

2.3.4. Degradation Assay—Microthread degradation was performed on single fibers on the bottom of 48 well plates as previously described [16]. Briefly, stretched microthreads were cut into 0.8 cm fragments and secured to the bottom of 48 well plates using medical grade silicone adhesive. Stock solutions of human plasmin (EMD Biosciences, San Diego, CA; 527621) were aliquoted and stored according to the manufacturer's instructions. Each experimental condition was run in triplicate. Microthreads were hydrated in 500 μL of TBS (25 mM Tris-HCl (Sigma), 0.9% NaCl, pH 7.5) for 1 hour, and images were taken with a 10× objective on a Leica inverted microscope (Leica, Wetzlar, Germany) coupled with Leica imaging software to record diameter values at time 0 (d_0). The TBS was aspirated and replaced with 500 μL of 0.1 U/mL of plasmin in TBS and samples were incubated at room temperature. Microthreads were imaged every 30 minutes or until they were completely degraded. Each image was processed with ImageJ (NIH) to measure the microthreads' diameter at three different positions along the length and plotted as a ratio to the initial diameter value (d/d_0).

2.4. Cell Culture

Immortalized mouse myoblasts (CRL-1772, ATCC, Manassas, VA; C2C12) were cultured in a 1:1 (v/v) ratio of high glucose Dulbecco's modified Eagle Medium (DMEM, Gibco BRL, Gaithersburg, MD) and Ham's F12 (Gibco), supplemented with 4 mM L-glutamine and 10% fetal bovine serum (FBS, HyClone, Logan, UT). Cells were incubated at 37 °C

with 5% CO_2 and maintained at a density below 70% confluence using standard cell culture techniques. Routine cell passage was conducted using 0.25% trypsin-EDTA (CellGro, Manassas, VA).

2.5. Cell Attachment and Alignment Assay

Two single microthreads from the same stretch group were adhered to stainless steel rings (Seastrom Manufacturing, Twin Falls ID; inner diameter 0.750 in.; outer diameter 1.188 in.; thickness 0.005 in.) with medical grade silicone adhesive. Each experimental condition was performed in duplicate. Individual rings were placed in wells of a standard six-well plate over an elevated 13 mm diameter circular Thermanox™ coverslip (Nalge Nunc International, Rochester, NY), as described previously [16, 17]. Prior to cell seeding, microthreads were sterilized in 70% ethanol for 1 hour, rinsed in DI water 3 times, air dried in a laminar flow hood, and stored in a desiccator until use.

Immediately prior to seeding, 150 μL of sterile PBS was added to the coverslip to hydrate the microthreads for at least 1 hour. To attach C2C12 cells to the microthread, the PBS was aspirated and replaced with 100 μL of cell suspension (100,000 cells/mL) in complete culture medium. After a four hour incubation, cell-seeded microthreads were transferred to a clean six-well plate with 2 mL of fresh medium and returned to the incubator. After 24 hours, threads were fixed in 4% paraformaldehyde and stained with Hoechst 33342 to visualize myoblast nuclei (Figure 8A). Fluorescent images were analyzed by thresholding the grey scale image in ImageJ (NIH) (Figure 8B), and performing the particle analysis function within the ImageJ software to obtain the orientation of the long axis of the nucleus with respect to the microthread (Figure 8C). Nuclei that were on the edge of the microthread, or in contact with another nucleus (cell-cell contact) were excluded from analysis, and the others were either binned in 15° increments and plotted into a histogram presenting the average frequency of each bin size, or averaged together to obtain total cell angle measurements.

2.6. Statistical Analyses

Statistical analyses were performed using a one-way analysis of variance (ANOVA) with $p < 0.05$ indicating significant differences between groups, using SigmaPlot 11.0 software. For post-hoc analyses, Holm-Sidak pairwise multiple comparison tests were performed to determine significant differences between experimental groups using an overall significance level of $p < 0.05$. Where indicated, a Student's t-test was performed with $p < 0.05$ indicating significant differences between groups. The data are reported as means ± standard deviation for the mechanical and structural characterization and as means ± standard error for the degradation (3 discrete threads were analyzed for each of six experimental runs) and cell alignment studies (4 discrete threads were analyzed for each condition for each of two experimental runs).

3. Results

3.1. Stretching Increases the Ultimate Tensile Strength of Fibrin Microthreads

The mechanical properties of static axially stretched microthreads were investigated for the design of tissue-specific microthread scaffolds. Characteristic stress-strain curves for stretched microthreads show that the 0, 50, and 75% stretch groups have an initial toe region of increasing elongation with little change in stress (Figure 2B). Interestingly, higher stretch percentages decreased this toe region, becoming undetectable in microthreads stretched 100% of their initial length, and also decreased the strain at failure (SAF) of the material twofold. Based on these mechanical results, we observed that the microthreads appear to exhibit 3 distinct structural morphologies that we are classifying as low stretch threads (threads stretched to 0, 50, or 75% of their initial length), moderate stretch threads (threads stretched to 100 or 125% of their initial length), or high stretch threads (threads stretched to 150, 175, or 200% of their initial length). Characteristic stress-strain curves of each of the low, moderate, and high stretch groups show the loss of the toe-region with the moderate and high stretch threads, as well as the increase in the maximum tangent modulus (MTM) with increasing stretch (Figure 2C). The mean diameters, peak loads, ultimate tensile strength (UTS), MTM, and SAF of all microthreads loaded to failure in uniaxial tension are summarized in Table 1. Ultimate tensile strengths (UTS) of high stretch threads were significantly higher than those of low stretch threads (Figure 3A). Additionally, moderate stretch threads displayed significantly lower UTS values than high stretch threads. The MTM values showed a similar trend where the high stretch threads were found to be stiffer than the low stretch threads (Figure 3B). High stretch microthreads also failed at significantly lower SAF values than low stretch microthreads (Figure 3C).

To characterize the relationship between static axial stretching and the stiffness of the fibrin threads, we analyzed the strain hardening behavior of the stretched microthreads. Strain hardening refers to an increase in the tangent modulus with increasing strain (compare initial and maximum tangent modulus in Figure 2A). Interestingly, static axial stretch was not found to affect the strain hardening ratio of fibrin microthreads (Table 2). Most stretching conditions demonstrated significantly higher MTM than the initial moduli in the toe regions of the stress-strain curves, showing that these fibrin microthreads are undergoing strain hardening. Additionally, the initial modulus of the high stretch threads was significantly greater than the initial modulus of low stretch threads. Combined with earlier observations about the effects of stretch on MTM values, these data suggest that high stretch threads are stiffer than low stretch threads at all strain values during uniaxial loading. Taken together, these data support the observation that there are three discrete ranges of mechanical strength that correspond to the amount of stretching of fibrin microthreads.

3.2. Stretching Decreases the Diameters and Swelling Ratios of Fibrin Microthreads, but does not Affect Poisson 's Ratio

To begin to understand the structural organization of fibrin fibrils within the microthreads, dried microthreads were imaged with a scanning electron microscope (SEM) and swelling ratios were calculated to estimate interfibrillar interactions, fibrillar packing and orientation as well as crosslinking density. Scanning electron micrographs of the microthreads show an

apparent decrease in diameter of the microthreads with increased stretch (Figure 4). Low stretch microthreads (Figure 4, 0% and 75%) exhibited a smooth, rounded morphology with no evidence of surface topography. With increasing stretch, the microthread surfaces exhibit a more complex topography. There is evidence of longitudinal grooves present on high stretch microthreads (Figure 4, 150% and 175%), suggesting that the uniaxial deformation generated by stretching of the microthreads may impart fibrillar reorganization on the surface of the microthreads (Figure 4, white arrows). Both the dry and wet diameters of microthreads were significantly higher in the low stretch thread groups compared to the high stretch groups (Figure 5A). The swelling ratios of low stretch threads were also significantly higher than high stretch groups (Figure 5B), suggesting that stretching microthreads decreases both their mean diameters and their swelling ratio. The transverse strain increased with increasing stretch (Figure 5C). High stretch microthreads had the highest transverse strain, and the low stretch threads had the lowest. Interestingly, Poisson's ratio was constant regardless of the amount of axial stretch applied to the microthreads (Figure 5D), suggesting that this material property is conserved through the stretch regimen applied in this study.

3.3. A Drying Phase is Necessary for the Increase in Ultimate Tensile Strength of Stretched Fibrin Microthreads

To investigate whether the microthread drying phase affected the stretching-mediated changes in the mechanical and structural properties of fibrin threads, we stretched microthreads immediately after extrusion and polymerization in the HEPES bath (Figure 1B). These microthreads were compared to those used in the previous experiment, where a drying step was included after polymerization, but prior to the stretching of the fibrin microthreads. When the UTS values of threads stretched immediately after polymerization were compared to corresponding threads that had undergone a drying phase prior to stretching, the groups with a drying phase had significantly higher UTS values (Figure 6). Additionally, threads stretched with a drying phase had smaller diameters than threads stretched immediately after polymerization, while 0% stretch threads had larger diameters than control threads (Table 3). Threads stretched immediately after polymerization also had comparable UTS values to the control microthreads. However, threads that were processed with a drying phase exhibited a fourfold increase in UTS with respect to control microthreads, demonstrating that the combination of a drying phase and stretching are necessary to enhance the mechanical strength of microthreads.

3.4. Stretch Does Not Affect the Proteolytic Degradation of Fibrin Microthreads

To evaluate whether static axial stretching affects the rate of proteolytic degradation of fibrin microthreads, microthreads were incubated with plasmin and the degradation of the microthreads was observed over time as a function of the change in microthread diameter. Since previous investigations showed a rapid rate of degradation of uncrosslinked fibrin microthreads [16], the kinetics of proteolytic degradation were slowed by performing the assay at room temperature. There was a trend for moderate and high stretch threads to have smaller d/d_0 ratios than low stretch threads at any point in time (Figure 7), however, no significant differences were observed in the degradation rate of low, moderate, or high stretch fibrin microthreads, based on d/d_0 measurements.

3.5. Stretch Enhances Cellular Alignment along the Longitudinal Axis of Fibrin Microthreads

We investigated how stretching fibrin microthreads affected cellular alignment of C2C12 myoblasts after seeding. All stretch percentages facilitated a range of cellular alignment with respect to the long axis of the microthread (Figure 8D). Cells tended to align more closely with the longitudinal axis of the microthreads with increasing levels of stretch, resulting in a 30% increase in myoblast nuclei oriented relative to low stretch threads (0-15° cell angle). The percentage of cells that showed no preferential orientation to the long axis of threads (45-90° cell angle) also decreased with increased stretch regimes (22%, 18%, and 4% for low, moderate, and high stretch threads, respectively). When the alignment angles of all of the cells were averaged together, there was almost a twofold, statistically significant decrease in cell orientation with respect to the long axis of the microthread (Figure 8E). Taken together, these data show that the surfaces of moderate and high stretch threads direct increased alignment of myoblast nuclei along the long axis of microthreads. This trend was most evident with myoblasts analyzed in the high stretch group, where a majority of cells were aligned within 15 degrees of the microthread axis, and had the least amount of cells aligned towards the circumferential axis of the microthreads.

4. Discussion

The goal of the present study was to characterize fibrin microthreads with tunable mechanical properties in the absence of exogenous crosslinking agents. Fibrin microthreads are a platform technology that can be used as scaffolds for tissue regeneration in a variety of tissue systems such as skeletal muscle, skin, tendon, ligament, or myocardium. Each of these tissue systems has distinct mechanical and structural requirements, suggesting that there is a significant need to create fibrin microthreads with tunable mechanical properties. In this study, we demonstrated that microthreads dried after polymerization, rehydrated, and then stretched to specific percentages produced three distinct stretch regimes (low, moderate or high stretch) that produce microthreads with specific mechanical properties. The tensile properties reported in this study for moderate and high stretch threads, are comparable to those previously reported for carbodiimide crosslinked fibrin microthreads [16]. High stretch fibrin microthreads have tensile strengths comparable to carbodiimide crosslinked microthreads in an acidic buffer (EDCa), and moderate stretch microthreads are comparable to carbodiimide crosslinked microthreads in a neutral buffer (EDCn). While UTS values of stretched microthreads were comparable to carbodiimide crosslinked microthreads, the stiffness of these microthreads increased three to fourfold in comparison to carbodiimide crosslinked threads.

Our observations that the tensile strength of fibrin microthreads increased with the magnitude of thread stretching are consistent with previous observations with collagen microthreads, where UTS and stiffness values of uncrosslinked collagen microthreads increased with static axial stretching [18]. Furthermore, when fibrin gels were stretched and imaged with atomic force microscopy, a significant increase in the interfibrillar alignment of fibrin fibrils was observed [14]. Interestingly, we did not observe any changes in Poisson's ratio with increasing stretch, suggesting that these microthreads, composed of a dense fibrin

matrix, demonstrated a consistent level of hydration within their fibrillar network, as previously suggested with low concentration fibrin gels [19]. Together with the swelling ratio observations, we hypothesize that the combination of static axial stretching and drying are affecting the ability of the microthreads to swell, independent of Poisson's ratio, resulting in decreased water content and subsequently increased packing density within the microthreads. These combined findings suggest that the increased tensile strength and stiffness of stretched microthreads is due to an increase in the interfibrillar orientation and interaction of fibrin fibrils within the microthread. An increase in the interfibrillar alignment would explain why no significant decreases in the load at failure were observed for stretched microthreads even when we observed decreases in the diameter of stretched fibrin microthreads.

When C2C12 myoblasts were seeded on the surfaces of stretched fibrin microthreads, we observed that cellular orientation appeared to sense changes in the topography on the surfaces of the scaffold. Small cylindrical substrates, such as fibrin microthreads, have been previously shown to facilitate longitudinal alignment of cells [8, 20]. This phenomenon may explain why approximately 40% of the myoblast nuclei were oriented with the longitudinal axis of low stretch microthreads (0-15° orientation). In this study, we observed that there was a shift in the overall distribution of cellular alignment towards the long axis of the scaffold when we applied a high stretch regime to the microthreads and further, that the mean alignment angle of cells seeded on stretched microthreads significantly decreased twofold. Additionally, it has been shown that increasing the alignment of fibers on the surface of a scaffold will enhance myoblast alignment along the scaffold [21]. Our SEM micrographs provide evidence of longitudinal topography on high stretch threads, further suggesting an alignment of the fibrils on the surface of the threads, similar to previous observations for stretched fibrin gels [14, 22]. Together, these findings support our hypothesis that static axial stretching of fibrin microthreads facilitates the reorganization and alignment of fibrin fibrils on the surfaces of scaffolds. To our knowledge, there has been little work on the design of scaffolds that concurrently mimic tissue-like fibrous architecture and also provide topographic instructive cues that direct cell function and orientation. In future studies, we will combine the findings presented here with an analysis on the topography of fibrin microthreads to assess the contribution of microthread topography to cell alignment, based on the hypothesis that the internal reorganization of fibrin fibrils within the microthread produces an aligned surface topography that facilitates enhanced cellular alignment.

It is interesting to note that static axially stretched fibrin microthreads show strain hardening ratios of 2-4, similar to previously reported values for uncrosslinked, single fibrin fibers [13]. Regardless of the amount of strain on the microthreads during uniaxial loading, there is a tenfold increase in stiffness between low and high stretch threads. Previous studies have shown that stiffer substrates stimulate myoblast proliferation, which may be important for delivering enough myoblasts to repair large muscle defects *in vivo* for skeletal muscle regeneration [23, 24]. In addition to increased alignment of fibrils on the surface of the scaffold, substrate stiffness has been suggested to enhance cell alignment, a critical step towards myoblast fusion [25]. While we have not characterized alignment-guided myoblast

differentiation on static axially stretched fibrin microthreads as a function of scaffold rigidity, we hypothesize that there would be an increased ability of stretched microthreads to support myoblast differentiation. Scaffold rigidity also plays a major role in cell migration [26, 27]. In future studies, we plan to systematically characterize the effect of microthread stiffness on cell migration and myoblast differentiation.

Previous studies showed that fibrin clots stretched 200-300% of their original length degraded at a slower rate, suggesting that stretching fibrin fibrils somehow blocked access of proteases to their target sites in fibrin [28]. In this study, we showed that fibrin microthreads, stretched 0-200% of their original length, generated scaffolds with tunable mechanical and morphologic properties without significantly changing the rate of proteolytic degradation of the materials. In previous studies, the density of fibrin fibrils has also been found to influence fibrinolysis, where densely packed, larger fibrils were found to degrade at slower rates than less densely packed, or thinner, fibrin fibrils [29, 30]. It is important to note that in these previous studies, researchers examined physiologic concentrations of fibrinogen. In our study, fibrin microthreads are extruded with a fibrinogen concentration that is almost tenfold higher than physiologic levels. We hypothesize that stretching these fibrin microthreads plastically deforms the fibrin fibril network within the microthread rather than protect discrete degradation sites. This mechanism may explain why we did not observe a significant change in the degradation rate of stretched threads.

When uncrosslinked microthreads were implanted in a large skeletal muscle defect, microthreads were shown to degrade within 1-2 weeks [31]. It was hypothesized that microthreads would have to persist for a longer duration of time for use as a scaffold in a large muscle defect. Static axial stretching of fibrin microthreads has not been found to significantly affect proteolytic degradation, so *in vivo* applications for these threads may be limited to implantation times of 1-2 weeks. Another application for fibrin microthreads has been to use microthreads as suture material, as well as a cell delivery vehicle [32]. We report here an efficient, and reproductive, method for increasing the mechanical strength of fibrin microthreads, which may aid in the use of these microthreads as a suture material due to their enhanced tensile strengths. The ability to stretch fibrin microthreads is also favorable from a manufacturing standpoint, as this method would increase the yield of usable microthreads per batch as well as standardize the microthread production process to reduce batch-to-batch variability. Further modifications of stretched microthreads, such as carbodiimide crosslinking, could generate microthreads with additional resistance to degradation as well as increased strength for use as a long-term scaffold for a variety of tissue regeneration applications.

5. Conclusions

In this study, we present fibrin microthreads that are dried, rehydrated, and then static axially stretched with low (0-75%), moderate (100-125%), or high (150-200%) stretch regimes to generate tunable mechanical properties such as UTS and stiffness. The increase in UTS was attributed to the drying phase as well as the decrease in microthread diameter, as failure loads did not change. Increased strengths were comparable to those of carbodiimide

crosslinked microthreads [16], demonstrating that crosslinking is not necessary to increase the mechanical strength of microthreads.

The fact that high stretch threads failed at the same load as low-stretch microthreads suggests that static axial stretching is reorganizing the fibrillar structure of fibrin fibrils within the microthreads. This hypothesis was supported by SEM micrographs and increased cellular alignment on high-stretch microthreads. Interestingly, stretched microthreads with increased mechanical strength did not have enhanced resistance to proteolytic degradation. Taken together, these findings suggest that we have developed a mechanism by which we can tune microthread structural properties without affecting their proteolytic degradation. Additionally, combining this process with crosslinking, or the incorporation of bioactive molecules, will significantly enhance the functional utility of these materials for the design of therapeutic delivery systems and scaffolds to promote functional tissue regeneration.

Acknowledgments

This research was funded in part by US Army (W81XWH-11-1-0631) and NIH R01-HL115282 (GDP) and NIH F31-DE023281 (JMG). The authors wish to thank Keith Gagnon for his technical assistance and Pat Flaherty for his help with the statistical analyses.

References

1. Pins GD, Christiansen DL, Patel R, Silver FH. Self-assembly of collagen fibers. Influence of fibrillar alignment and decorin on mechanical properties. Biophysical journal. 1997; 73:2164–72. [PubMed: 9336212]
2. Cornwell KG, Lei P, Andreadis ST, Pins GD. Crosslinking of discrete self-assembled collagen threads: Effects on mechanical strength and cell-matrix interactions. J Biomed Mater Res A. 2007; 80:362–71. [PubMed: 17001644]
3. Zeugolis DI, Paul GR, Attenburrow G. Cross-linking of extruded collagen fibers--a biomimetic three-dimensional scaffold for tissue engineering applications. J Biomed Mater Res A. 2009; 89:895–908. [PubMed: 18465819]
4. Chen J, Altman GH, Karageorgiou V, Horan R, Collette A, Volloch V, et al. Human bone marrow stromal cell and ligament fibroblast responses on RGD-modified silk fibers. J Biomed Mater Res A. 2003; 67:559–70. [PubMed: 14566798]
5. Horan RL, Antle K, Collette AL, Wang Y, Huang J, Moreau JE, et al. In vitro degradation of silk fibroin. Biomaterials. 2005; 26:3385–93. [PubMed: 15621227]
6. Horan RL, Collette AL, Lee C, Antle K, Chen J, Altman GH. Yarn design for functional tissue engineering. Journal of biomechanics. 2006; 39:2232–40. [PubMed: 16182301]
7. Cornwell KG, Downing BR, Pins GD. Characterizing fibroblast migration on discrete collagen threads for applications in tissue regeneration. J Biomed Mater Res A. 2004; 71:55–62. [PubMed: 15368254]
8. Cornwell KG, Pins GD. Enhanced proliferation and migration of fibroblasts on the surface of fibroblast growth factor-2-loaded fibrin microthreads. Tissue Eng Part A. 2010; 16:3669–77. [PubMed: 20673132]
9. Turner NJ, Badylak SF. Regeneration of skeletal muscle. Cell Tissue Res. 2012; 347:759–74. [PubMed: 21667167]
10. Clark RA. Fibrin and wound healing. Ann N Y Acad Sci. 2001; 936:355–67. [PubMed: 11460492]
11. Brown AC, Barker TH. Fibrin-based biomaterials: Modulation of macroscopic properties through rational design at the molecular level. Acta biomaterialia. 2013
12. Grassl ED, Oegema TR, Tranquillo RT. Fibrin as an alternative biopolymer to type-I collagen for the fabrication of a media equivalent. Journal of Biomedical Materials Research. 2002; 60:607–12. [PubMed: 11948519]

13. Liu W, Carlisle CR, Sparks EA, Guthold M. The mechanical properties of single fibrin fibers. J Thromb Haemost. 2010; 8:1030–6. [PubMed: 20088938]
14. Matsumoto T, Sasaki J, Alsberg E, Egusa H, Yatani H, Sohmura T. Three-dimensional cell and tissue patterning in a strained fibrin gel system. PLoS ONE. 2007; 2:e1211. [PubMed: 18030345]
15. Cornwell KG, Pins GD. Discrete crosslinked fibrin microthread scaffolds for tissue regeneration. J Biomed Mater Res A. 2007; 82:104–12. [PubMed: 17269139]
16. Grasman JM, Page RL, Dominko T, Pins GD. Crosslinking strategies facilitate tunable structural properties of fibrin microthreads. Acta Biomaterialia. 2012; 8:4020–30. [PubMed: 22824528]
17. Proulx MK, Carey SP, Ditroia LM, Jones CM, Fakharzadeh M, Guyette JP, et al. Fibrin microthreads support mesenchymal stem cell growth while maintaining differentiation potential. J Biomed Mater Res A. 2011; 96:301–12. [PubMed: 21171149]
18. Pins GD, Huang EK, Christiansen DL, Silver FH. Effects of static axial strain on the tensile properties and failure mechanisms of self-assembled collagen fibers. J Appl Polym Sci. 1997; 63:1429–40.
19. Lai VK, Lake SP, Frey CR, Tranquillo RT, Barocas VH. Mechanical behavior of collagen-fibrin co-gels reflects transition from series to parallel interactions with increasing collagen content. Journal of Biomechanical Engineering. 2012; 134:011004. [PubMed: 22482659]
20. Rovensky YA, Samoilov VI. Morphogenetic response of cultured normal and transformed ibroblasts, and epitheliocytes, to a cylindrical substratum surface. J of Cell Science. 1994; 107:1255–63. [PubMed: 7929633]
21. Choi JS, Lee SJ, Christ GJ, Atala A, Yoo JJ. The influence of electrospun aligned poly(epsilon-caprolactone)/collagen nanofiber meshes on the formation of self-aligned skeletal muscle myotubes. Biomaterials. 2008; 29:2899–906. [PubMed: 18400295]
22. Brown AE, Litvinov RI, Discher DE, Purohit PK, Weisel JW. Multiscale mechanics of fibrin polymer: gel stretching with protein unfolding and loss of water. Science. 2009; 325:741–4. [PubMed: 19661428]
23. Boontheekul T, Hill EE, Kong HJ, Mooney DJ. Regulating myoblast phenotype through controlled gel stiffness and degradation. Tissue engineering. 2007; 13:1431–42. [PubMed: 17561804]
24. Gilbert PM, Havenstrite KL, Magnusson KE, Sacco A, Leonardi NA, Kraft P, et al. Substrate elasticity regulates skeletal muscle stem cell self-renewal in culture. Science. 2010; 329:1078–81. [PubMed: 20647425]
25. Engler AJ, Griffin MA, Sen S, Bonnemann CG, Sweeney HL, Discher DE. Myotubes differentiate optimally on substrates with tissue-like stiffness: pathological implications for soft or stiff microenvironments. The Journal of Cell Biology. 2004; 166:877–87. [PubMed: 15364962]
26. Tse JR, Engler AJ. Stiffness gradients mimicking in vivo tissue variation regulate mesenchymal stem cell fate. PLoS ONE. 2011; 6:e15978. [PubMed: 21246050]
27. Isenberg BC, Dimilla PA, Walker M, Kim S, Wong JY. Vascular smooth muscle cell durotaxis depends on substrate stiffness gradient strength. Biophysical journal. 2009; 97:1313–22. [PubMed: 19720019]
28. Varju I, Sotonyi P, Machovich R, Szabo L, Tenekedjiev K, Silva MM, et al. Hindered dissolution of fibrin formed under mechanical stress. J Thromb Haemost. 2011; 9:979–86. [PubMed: 21251205]
29. Collet JP, Lesty C, Montalescot G, Weisel JW. Dynamic changes of fibrin architecture during fibrin formation and intrinsic fibrinolysis of fibrin-rich clots. The Journal of biological chemistry. 2003; 278:21331–5. [PubMed: 12642590]
30. Undas A, Zalewski J, Krochin M, Siudak Z, Sadowski M, Pregowski J, et al. Altered plasma fibrin clot properties are associated with in-stent thrombosis. Arteriosclerosis, thrombosis, and vascular biology. 2010; 30:276–82.
31. Page RL, Malcuit C, Vilner L, Vojtic I, Shaw S, Hedblom E, et al. Restoration of skeletal muscle defects with adult human cells delivered on fibrin microthreads. Tissue Eng Part A. 2011; 17:2629–40. [PubMed: 21699414]
32. Guyette JP, Fakharzadeh M, Burford EJ, Tao ZW, Pins GD, Rolle MW, et al. A novel suture-based method for efficient transplantation of stem cells. J Biomed Mater Res A. 2013; 101:809–18. [PubMed: 22961975]

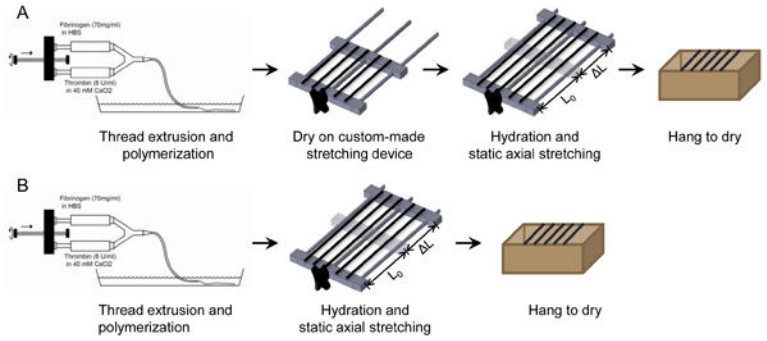

Figure 1.

A flow-chart of the experimental setup for microthread fabrication with (A) and without (B) a drying phase. Threads are first extruded into a pH controlled bath solution and incubated for 10 minutes at room temperature for microthread polymerization. After polymerization, threads are removed from the bath and dried overnight on a custom-made stretching device. The next day the threads are rehydrated, static axially stretched to the desired percentage, and dried for immediate testing or storage (A). Control microthreads were immediately stretched after fibrin polymerization and dried overnight (B).

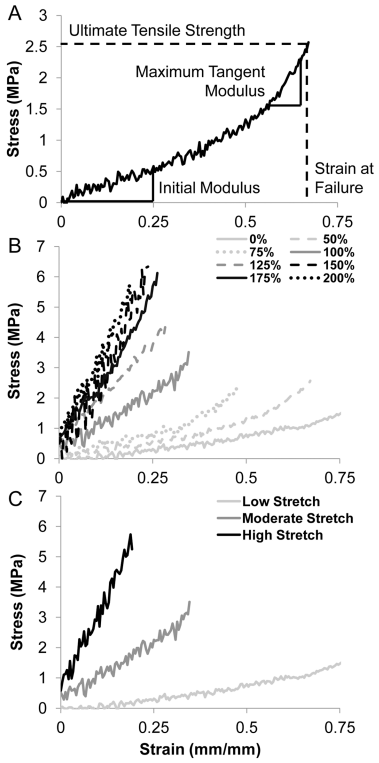

Figure 2.

Characteristic stress-strain curves for fibrin microthreads fabricated with a drying phase. Microthreads were produced and dried, rehydrated in DI water, and stretched to the indicated percentage. (A) A representative stress-strain curve showing how each mechanical parameter was calculated in our MATLAB script. (B) Microthreads that were stretched 0-75% of their original lengths displayed elastic toe regions and low stiffness. Higher stretch groups (100 – 200%) did not always have characteristic toe-regions, but they appeared to deform linearly until failure at higher stresses and at lower strain values. (C) Representative stress-strain curves from low stretch threads (stretched 0, 50, or 75% of their initial lengths), moderate stretch threads (stretched 100 or 125% of their initial lengths), and high stretch threads (stretched 150, 175, 200% of their initial lengths). Moderate and high stretch threads do not exhibit a toe-region, but exhibit linear elastic slopes of their stress-strain curves.

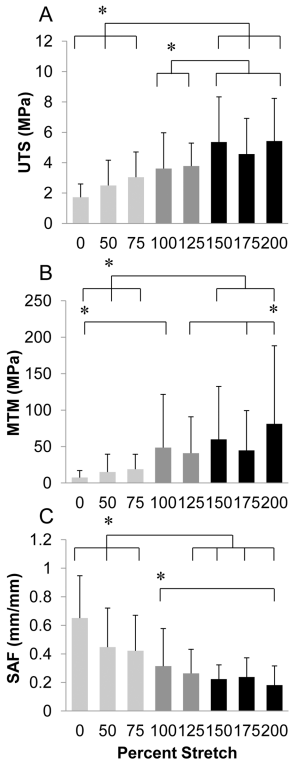

Figure 3.

Mechanical properties of fibrin microthreads as a function of stretch percentage. Microthreads were fabricated and dried, rehydrated in DI water, stretched to the indicated percentage and dried in their stretched state. Microthreads were subsequently pulled to failure under uniaxial tension and the (A) ultimate tensile strength (UTS), (B) maximum tangent modulus (MTM), and (C) strain at failure (SAF) were calculated. Low stretch threads (stretched 0, 50, or 75% of their initial lengths) failed at significantly lower UTS values, and were less stiff than high stretch threads (stretched 150, 175, or 200% of their initial lengths). Low stretch threads also failed at significantly higher strain values than high stretch threads. * indicates statistical significance between corresponding groups using one-way ANOVA with Holm- Sidak post hoc analysis ($p < 0.05$, $n \geq 41$).

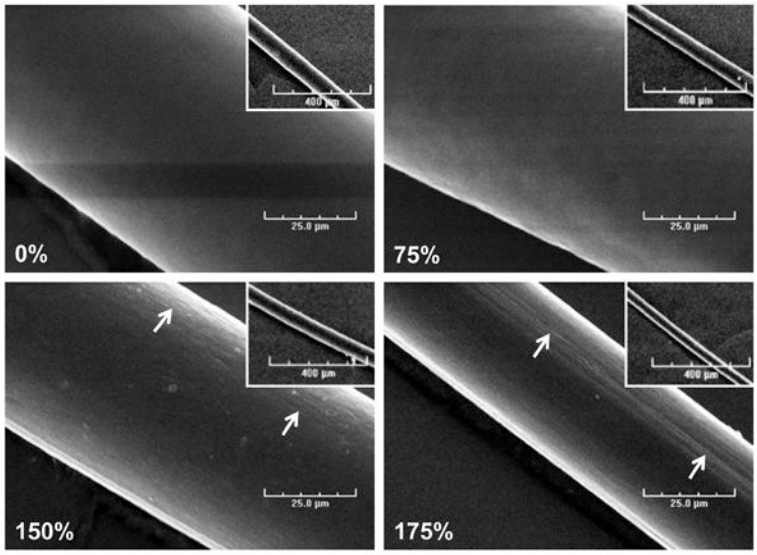

Figure 4.

Low (inset) and high magnification scanning electron micrographs of fibrin microthreads stretched 0%, 75%, 150%, and 175% of their original lengths. As microthreads are stretched, their diameters decrease, and the topography changes from a smooth surface (0% and 75% stretch threads) to a surface with aligned grooves present at the 150% and 175% stretch groups (white arrows). Scale bar is 25 μm and the scale on the inset image is 400 μm.

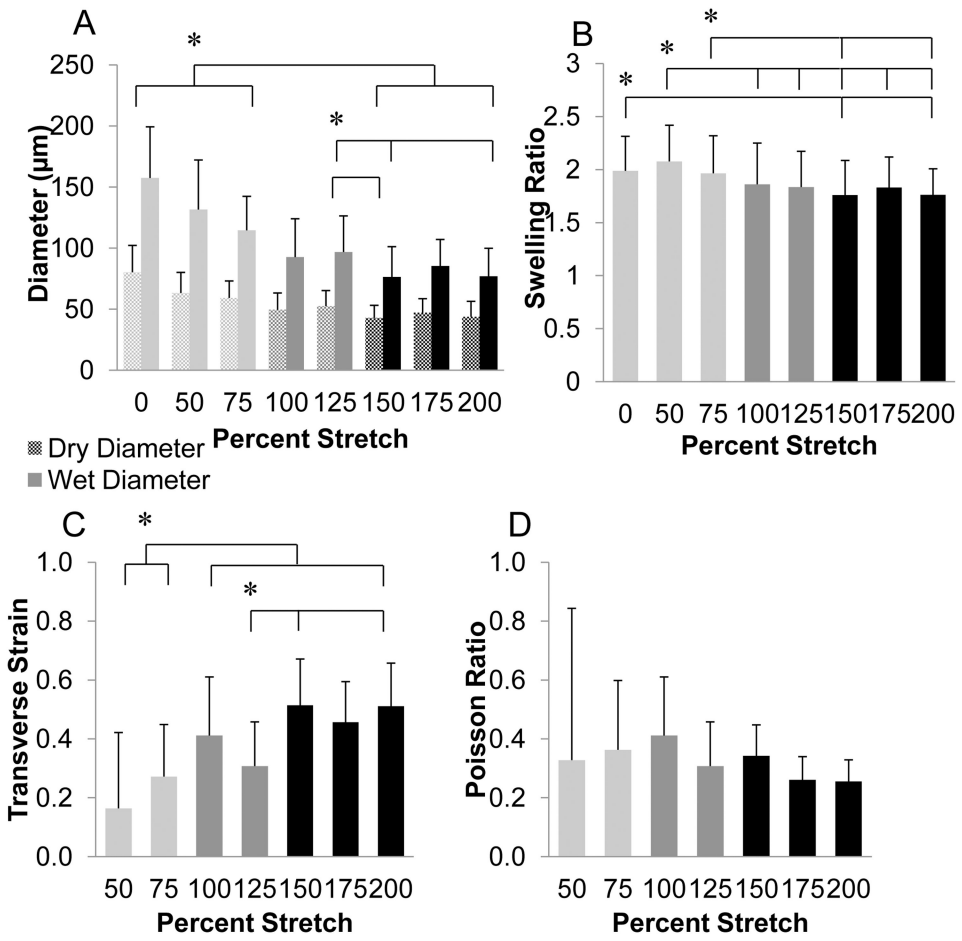

Figure 5.

Structural properties of fibrin microthreads as a function of stretch. (A) Plot showing changes of wet and dry diameters of static axially stretched microthreads. Low stretch microthreads had significantly larger diameters than high stretch microthreads. (B) Plot showing changes in swelling ratios of microthreads as a function of stretch. Low stretch microthreads had significantly higher swelling ratios than high stretch microthreads. (C) Plot showing the transverse strain along the diameter of stretched microthreads. The low stretch regimen resulted in transverse strain measurements that were significantly lower than all other stretch regimens. (D) Plot showing Poisson's ratio, which was found to be constant regardless of the amount of axial stretch applied to the microthreads. * indicates statistical significance between corresponding groups using one-way ANOVA with Holm- Sidak post hoc analysis ($p < 0.05$, $n \geq 41$).

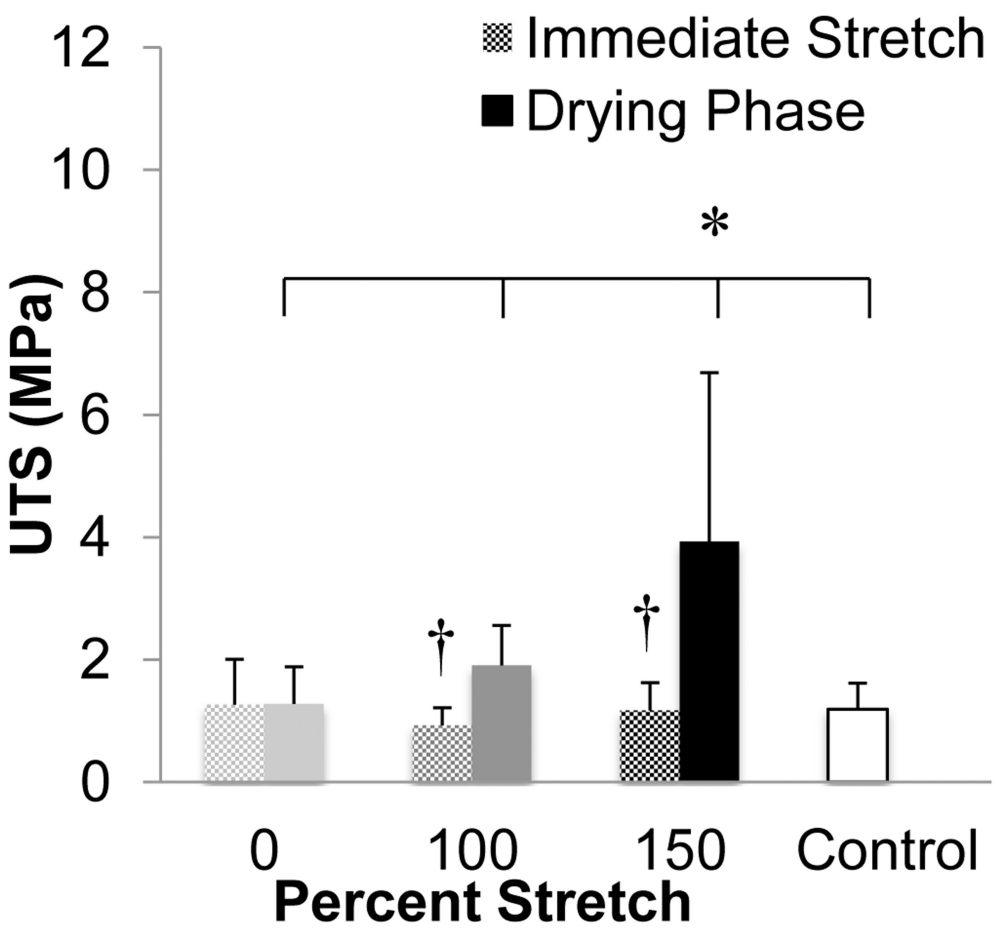

Figure 6.

Comparison of the ultimate tensile strengths (UTS) of fibrin microthreads stretched with a drying phase or stretched immediately after fibrin polymerization (immediate stretch). The UTS values of threads stretched with a drying phase were significantly higher than threads that were immediately stretched after polymerization. Additionally, microthreads stretched 150% with a drying phase had significantly higher UTS values than any other group, including the control. * indicates significance between corresponding groups and † indicates significance between immediate stretch and drying phase treatments within a single percentage group as determined by one-way ANOVA with Holm-Sidak post hoc analysis and a Student's t-test to compare results between immediate stretch and drying phase threads of the same stretch percentage ($p < 0.05$, $n \geq 25$).

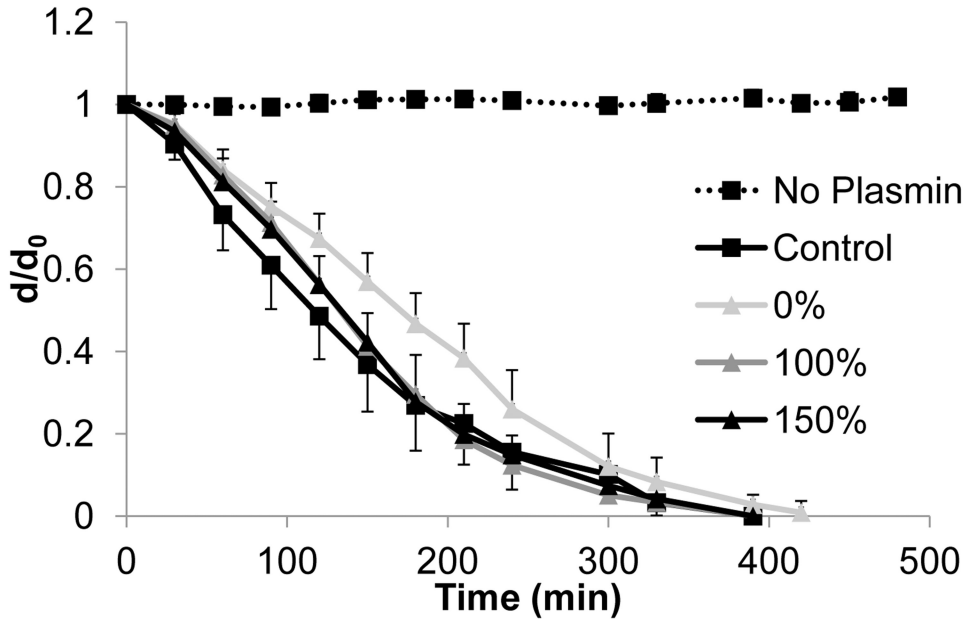

Figure 7.

Degradation profiles of stretched microthreads fabricated with a drying phase treated with plasmin. Plots show changes in microthread diameter as a function of time and stretching regime. Results were compared to the threads fabricated with the current fabrication process (control), and mic rothreads incubated without plasmin (no plasmin). While 0% stretch threads exhibited a lag in the initial rate of degradation with respect to 100 and 150% stretch threads as indicated by a smaller negative slope of d/d_0 versus time, none of these degradation profiles are statistically different from one another. Data are presented as the mean ± standard error (n=6).

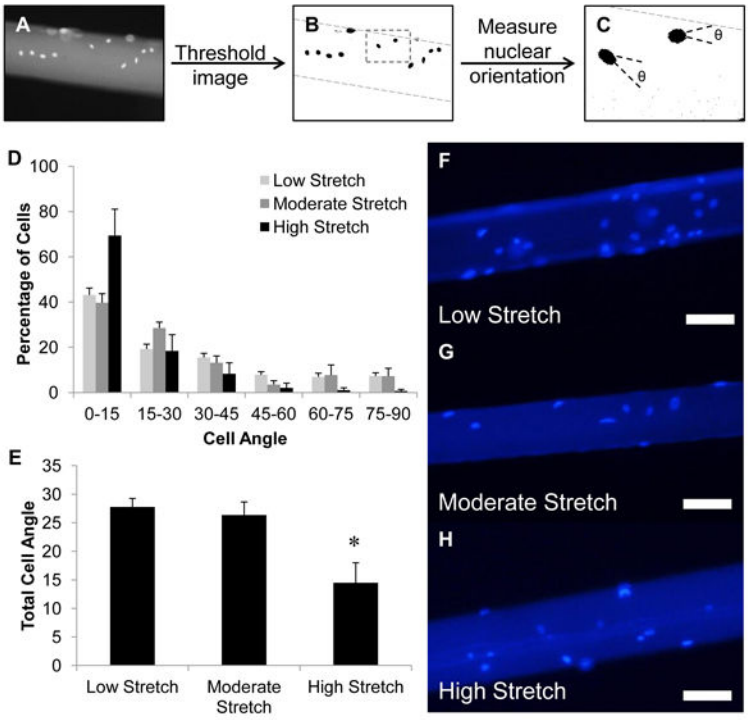

Figure 8.

C2C12 myoblast alignment on static axially stretched fibrin microthreads. Myoblast nuclei were visualized with Hoechst 33342 and imaged with an inverted microscope. Grey scale images of nuclei on microthreads (A), were thresholded to remove background fluorescence and to visualize nuclei in ImageJ (B), and the ImageJ function analyze particles was used to identify individual nuclei and their orientation with respect to the long axis of the microthread (C). Results from the analysis on nuclear alignment of myoblasts along each microthread are presented as histograms showing the average percentage of nuclei oriented along the long axis of microthreads in 15° increments (D). In all cases, most nuclei were aligned with the long axis of the microthread (0-15° orientation). There was no change in the amount of cells aligned with the long axis of the microthread between low and moderate stretch thread groups, however, there was almost a twofold increase with high stretch threads. The average alignment angle of all nuclei along the microthreads shows that the average nuclear angle decreased twofold when cultured on high stretch threads (E). Representative fluorescent images showing Hoechst stained nuclei on stretched microthreads show similar levels of attachment on threads regardless of their stretch regime (F-H). * indicates significance with all other groups as determined by one-way ANOVA with Holm-Sidak post hoc analysis ($p < 0.05$, $n \geq 150$ cells analyzed for each group, $n \geq 2$ for experimental duplicates, scale = 100 μm).

Table 1

The mechanical and structural properties of fibrin microthreads stretched after a drying phase. Data is presented as mean ± standard deviation.

Stretch Percent	Sample Size	Diameter (μm)		Swelling Ratio	UTS (MPa)	MTM (MPa)	SAF (mm/mm)	Load (mN)
		Dry	Wet					
0%	50	80 ± 22	157 ± 42	2.0 ± 0.3	1.7 ± 0.9	7.5 ± 9.7	0.651 ± 0.287	34 ± 26
50%	51	63 ± 17	132 ± 41	2.1 ± 0.3	2.5 ± 1.7	15.0 ± 24.5	0.447 ± 0.274	29 ± 30
75%	59	59 ± 14	115 ± 28	2.0 ± 0.3	3.0 ± 1.7	18.9 ± 20.5	0.422 ± 0.248	30 ± 19
100%	43	50 ± 14	93 ± 31	1.9 ± 0.4	3.6 ± 2.4	48.6 ± 72.6	0.314 ± 0.264	26 ± 31
125%	41	53 ± 13	97 ± 30	1.8 ± 0.3	3.8 ± 1.5	41.0 ± 49.8	0.264 ± 0.168	29 ± 18
150%	44	43 ± 10	77 ± 25	1.8 ± 0.3	5.4 ± 3.0	59.8 ± 72.8	0.224 ± 0.099	22 ± 12
175%	58	47 ± 11	86 ± 22	1.8 ± 0.3	4.6 ± 2.4	44.7 ± 54.5	0.238 ± 0.134	27 ± 15
200%	47	44 ± 13	77 ± 23	1.8 ± 0.2	5.4 ± 2.8	81.1 ± 107.1	0.182 ± 0.134	24 ± 12

Table 2

Strain hardening behavior of static uniaxially stretched fibrin microthreads. Microthreads were pulled to failure under uniaxial tension and the stress-strain plots were analyzed for the initial modulus and the maximum tangent modulus (MTM). The strain hardening ratio is defined as the ratio between the MTM and the initial modulus. Data is presented as mean ± standard deviation.

Stretch Percent (%)	Initial Modulus (MPa)	MTM (MPa)	Strain Hardening Ratio
0	2.2 ± 1.6‡	7.5 ± 9.7	3.9 ± 4.6
50	7.6 ± 9.0†	15.0 ± 24.5	2.7 ± 1.0
75	6.6 ± 5.2‡†	18.9 ± 20.5	3.0 ± 1.3
100	22.3 ± 33.9*	48.6 ± 73.0	4.7 ± 7.3
125	13.3 ± 8.8‡	41.0 ± 49.8	4.2 ± 6.8
150	17.8 ± 18.3‡	59.8 ± 72.7	4.3 ± 7.8
175	21.5 ± 35.7‡*	44.7 ± 54.5	3.8 ± 4.9
200	30.9 ± 22.4‡*	81.1 ± 107.1	2.7 ± 1.5

*indicates significance with the 0% stretch group and

†indicates significance with the 200% stretch group as determined by one-way ANOVA with Holm-Sidak post hoc analysis, and

‡indicates significance between initial modulus and MTM within a single percentage group as determined by Student's t-test ($p < 0.05$, $n \geq 41$).

Table 3

The mechanical properties of fibrin microthreads stretched with a drying phase compared to threads stretched immediately after fibrin polymerization and to the current fabrication process (Control). Data is presented as mean ± standard deviation.

Stretch Percent	Drying Phase	Sample Size	Diameter (μm)		UTS (MPa)	Load (mN)	SAF (mm/mm)
			Dry	Wet			
Control	-	33	54 ± 11	130 ± 22	1.2 ± 0.4	15 ± 4	0.492 ± 0.239
0%	+	29	68 ± 16*	156 ± 33*	1.3 ± 0.6	23 ± 11*	0.899 ± 0.217*
0%	-	34	69 ± 10*	164 ± 21*	1.3 ± 0.7	27 ± 18*	0.755 ± 0.318*
100%	+	31	42 ± 9*	97 ± 17*	1.9 ± 0.7	13 ± 4	0.419 ± 0.136
100%	-	31	48 ± 8*†	132 ± 13†	0.9 ± 0.3†	12 ± 3	0.669 ± 0.130*†
150%	+	32	47 ± 13*	100 ± 37*	3.9 ± 2.8*	23 ± 9*	0.487 ± 0.235
150%	-	25	47 ± 9*	123 ± 21†	1.2 ± 0.5†	13 ± 4†	0.546 ± 0.141

† indicates statistical significance from threads stretched with a drying phase determined with a Student's t-test ($p < 0.05$) and

* indicates statistical significance from control threads using one-way ANOVA with Holm- Sidak post hoc analysis ($p < 0.05$).